LETTER

doi:10.1038/nature12240

Innate lymphoid cells regulate CD4$^+$ T-cell responses to intestinal commensal bacteria

Matthew R. Hepworth[1,2], Laurel A. Monticelli[2,3], Thomas C. Fung[1,2,3], Carly G. K. Ziegler[4], Stephanie Grunberg[3], Rohini Sinha[3], Adriana R. Mantegazza[5], Hak-Ling Ma[6], Alison Crawford[2,3], Jill M. Angelosanto[2,3], E. John Wherry[2,3], Pandelakis A. Koni[7], Frederic D. Bushman[3], Charles O. Elson[8], Gérard Eberl[9,10], David Artis[2,3,11] & Gregory F. Sonnenberg[1,2]

Innate lymphoid cells (ILCs) are a recently characterized family of immune cells that have critical roles in cytokine-mediated regulation of intestinal epithelial cell barrier integrity[1–10]. Alterations in ILC responses are associated with multiple chronic human diseases, including inflammatory bowel disease, implicating a role for ILCs in disease pathogenesis[3,8,11–13]. Owing to an inability to target ILCs selectively, experimental studies assessing ILC function have predominantly used mice lacking adaptive immune cells[1–10]. However, in lymphocyte-sufficient hosts ILCs are vastly outnumbered by CD4$^+$ T cells, which express similar profiles of effector cytokines. Therefore, the function of ILCs in the presence of adaptive immunity and their potential to influence adaptive immune cell responses remain unknown. To test this, we used genetic or antibody-mediated depletion strategies to target murine ILCs in the presence of an adaptive immune system. We show that loss of retinoic-acid-receptor-related orphan receptor-γt-positive (RORγt$^+$) ILCs was associated with dysregulated adaptive immune cell responses against commensal bacteria and low-grade systemic inflammation. Remarkably, ILC-mediated regulation of adaptive immune cells occurred independently of interleukin (IL)-17A, IL-22 or IL-23. Genome-wide transcriptional profiling and functional analyses revealed that RORγt$^+$ ILCs express major histocompatibility complex class II (MHCII) and can process and present antigen. However, rather than inducing T-cell proliferation, ILCs acted to limit commensal bacteria-specific CD4$^+$ T-cell responses. Consistent with this, selective deletion of MHCII in murine RORγt$^+$ ILCs resulted in dysregulated commensal bacteria-dependent CD4$^+$ T-cell responses that promoted spontaneous intestinal inflammation. These data identify that ILCs maintain intestinal homeostasis through MHCII-dependent interactions with CD4$^+$ T cells that limit pathological adaptive immune cell responses to commensal bacteria.

ILCs are a heterogeneous population of innate immune cells that can be grouped based on their expression of, and developmental requirements for, specific transcription factors and cytokines[1,8–10]. Group 1 ILCs depend on T-bet and express interferon (IFN)-γ, whereas group 2 ILCs depend on ROR-α and GATA3 and express IL-5, IL-13 and amphiregulin[1,8–10]. Group 3 ILCs critically depend on RORγt for their development and in response to IL-23 stimulation produce the effector cytokines IL-17A and IL-22, which directly regulate innate immunity, inflammation and anatomical containment of pathogenic and commensal bacteria in the intestine[1,8–10,14]. However, the function of group 3 ILCs in the presence of adaptive immunity, and whether ILCs can influence adaptive immune cell responses, is unknown. To test this, adaptive immune cell responses were examined in mice lacking RORγt (*Rorc*$^{gfp/gfp}$). In comparison to control mice, *Rorc*$^{gfp/gfp}$ mice exhibited significantly increased frequencies of peripheral proliferating Ki-67$^+$CD4$^+$ T cells and effector/effector memory CD44^{high}CD62L^{low}CD4$^+$ T cells (Fig. 1a) and developed splenomegaly (Fig. 1b, c), indicative of disrupted immune cell homeostasis. *Rorc*$^{gfp/gfp}$ mice also exhibited elevated levels of commensal bacteria-specific serum IgG (Fig. 1d), suggesting that commensal bacteria were promoting activation of adaptive immune cells in the absence of RORγt. Consistent with this, oral administration of antibiotics to *Rorc*$^{gfp/gfp}$ mice was associated with significantly reduced peripheral Ki-67$^+$CD4$^+$ T cells and CD44^{high}CD62L^{low}CD4$^+$ T cells, spleen size and weight and commensal bacteria-specific serum IgG (Fig. 1a–d). As T cells also express RORγt and RORγt-deficient mice exhibit several developmental abnormalities[6,15,16], we used CD90-disparate chimaeras to allow transient depletion of CD90.2$^+$ ILCs, but not CD90.1$^+$ T cells[3,7]. Depletion of ILCs in CD90-chimaeric mice with an anti-CD90.2 monoclonal antibody resulted in significantly increased frequencies of dysregulated CD4$^+$ T cells, increased spleen weight and elevated commensal bacteria-specific serum IgG responses (Supplementary Fig. 1a–d), suggesting a critical role for ILCs in the regulation of inflammatory adaptive immune cell responses to commensal bacteria. Unexpectedly, IL-22-, IL-17A- and IL-23-deficient mice did not exhibit altered CD4$^+$ T-cell responses, splenomegaly or elevated levels of commensal bacteria-specific serum IgG (Supplementary Fig. 2a–c). Furthermore, transient blockade of IL-22, IL-17A, IL-23 or IL-17RA in C57BL/6 mice also failed to exacerbate adaptive immune cell responses to commensal bacteria (Supplementary Fig. 2d–i), indicating that ILCs regulate adaptive immune cell responses independently of effector cytokines.

To identify the mechanisms by which RORγt$^+$ group 3 ILCs regulate commensal bacteria-responsive adaptive immune cells, genome-wide transcriptional profiles of RORγt$^+$ ILCs were compared to those of naive CD4$^+$ T cells (Fig. 1e, f). Analysis of the top differentially expressed transcripts in RORγt$^+$ group 3 ILCs revealed a significant enrichment for genes involved in pathways of 'haematopoietic or lymphoid organ development' and 'immune response' (Fig. 1e), consistent with previous analyses of RORγt$^+$ ILCs[17,18]. Notably, an additional pathway that was highly enriched in the transcriptional profile of group 3 ILCs was 'antigen processing and presentation of peptide antigen via MHCII' (Fig. 1e). Indeed, relative to naive CD4$^+$ T cells (Fig. 1f) and previously published arrays of *in-vitro*-generated T-helper 17 cells[19] (Supplementary Fig. 3), group 3 ILCs were highly enriched in transcripts involved in MHCII antigen processing and presentation pathways, such as *Cd74*, *H2-DMb2*, *H2-DMa*, *H2-Ab1* and *H2-Aa*. Consistent with these transcriptional analyses, MHCII

[1]Division of Gastroenterology, Department of Medicine, Perelman School of Medicine, University of Pennsylvania, Philadelphia, Pennsylvania 19104, USA. [2]Institute for Immunology, Perelman School of Medicine, University of Pennsylvania, Philadelphia, Pennsylvania 19104, USA. [3]Department of Microbiology, Perelman School of Medicine, University of Pennsylvania, Philadelphia, Pennsylvania 19104, USA. [4]ImmunoDynamics Group, Programs in Computational Biology and Immunology, Memorial Sloan-Kettering Cancer Center, New York, New York 10065, USA. [5]Department of Pathology and Laboratory Medicine, and Department of Physiology, Perelman School of Medicine, University of Pennsylvania, Philadelphia, Pennsylvania 19104, USA. [6]Inflammation and Immunology Research Unit, Biotherapeutics Research and Development, Pfizer Worldwide R&D, Cambridge, Massachusetts 02140, USA. [7]Cancer Immunology, Inflammation & Tolerance Program, Georgia Health Sciences University Cancer Center, Augusta, Georgia 30912, USA. [8]Department of Medicine, University of Alabama at Birmingham, Birmingham, Alabama 35294, USA. [9]Lymphoid Tissue Development Unit, Institute Pasteur, 75724 Paris, France. [10]Centre National de la Recherche Scientifique, URA 1961, 75724 Paris, France. [11]Department of Pathobiology, School of Veterinary Medicine, University of Pennsylvania, Philadelphia, Pennsylvania 19104, USA.

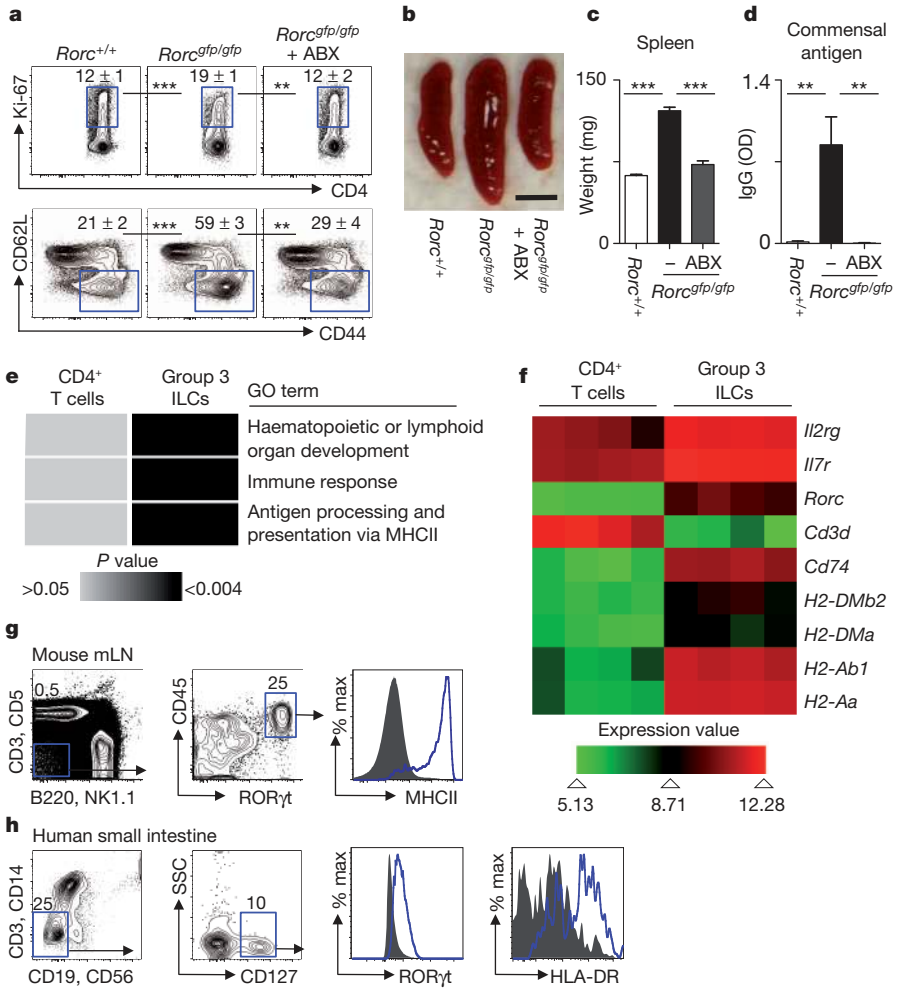

Figure 1 | RORγt$^+$ ILCs regulate adaptive immune cell responses to commensal bacteria and are enriched in MHCII-associated genes. **a**–**d**, Defined age- and sex-matched mouse strains were examined for the frequency of splenic Ki-67$^+$CD4$^+$ T cells (top) and CD44^{high}CD62L^{low}CD4$^+$ T cells (bottom) (**a**), spleen size (**b**), spleen weight (**c**) and relative absorbance values (OD) of serum IgG specific to commensal bacteria (**d**). Antibiotics (ABX) were administered in the drinking water from weaning until 6–8 weeks of age. Scale bar, 0.5 cm (**b**). Flow cytometry plots are gated on live CD4$^+$CD3$^+$ T cells (**a**). **e**, **f**, DAVID pathway analysis of GO terms enriched in the transcriptional profiles of naive CD4$^+$ T cells and group 3 RORγt$^+$ ILCs (**e**) and heat map of selected lymphoid-associated and MHCII-associated gene transcripts (**f**). **g**, **h**, Gating strategy for ILCs and expression of RORγt and MHCII in ILCs from the mesenteric lymph node (mLN) of naive RORγt–eGFP reporter mice (**g**) and the small intestine of healthy humans (**h**). Blue line, ILCs; grey fill, negative control population. Data are representative of three independent experiments containing 3–5 mice per group or four human donors. Results are shown as the means ± s.e.m. $^{**}P < 0.01$, $^{***}P < 0.001$ (two-tailed Student's *t*-test).

protein was detected on gated lineage$^-$CD45$^+$RORγt$^+$ ILCs from the mesenteric lymph node of naive RORγt–eGFP reporter mice (Fig. 1g). Critically, MHCII protein was also identified on gated lineage$^-$CD127$^+$RORγt$^+$ ILCs from the small intestine of healthy humans (Fig. 1h). Collectively, these results indicate that group 3 RORγt$^+$ ILCs in the intestinal and lymphoid tissues of healthy mice and humans express MHCII.

To interrogate whether MHCII expression was restricted to group 3 ILCs, total lineage$^-$CD45$^+$CD90.2$^+$ ILCs in the murine small intestine were subdivided into group 1, 2 and 3 ILCs by expression of their defining transcription factors (Fig. 2a, b and Supplementary Fig. 4a–e). Group 1 ILCs (RORγt$^-$T-bet$^+$NKp46$^{+/-}$) were found to lack MHCII expression (Supplementary Fig. 4d–f), whereas group 2 ILCs (GATA-3$^+$) expressed intermediate levels of MHCII (Supplementary Fig. 4c). Microarray analyses confirmed the enrichment of MHCII-associated genes in group 3 ILCs versus previously published arrays of group 1 ILCs, such as natural killer (NK) cells[20] (Supplementary Fig. 5a) and group 2 ILCs[17] (Supplementary Fig. 5b). Significant heterogeneity exists within RORγt$^+$ group 3 ILCs and three subgroups can be identified on the basis of expression of NKp46 and T-bet (Fig. 2a)[9,10,21]. MHCII was found to be highly expressed on RORγt$^+$ ILCs that lacked expression of both T-bet and NKp46, whereas minimal expression of MHCII was observed on RORγt$^+$T-bet$^+$NKp46$^-$ and RORγt$^+$T-bet$^+$NKp46$^+$ ILC subsets (Fig. 2b) isolated from the small intestine of naive mice. Consistent with this, previously published microarray data profiling ILCs based on NKp46 and RORγt expression[18] also revealed an enrichment of MHCII-associated genes in RORγt$^+$ ILCs that lacked NKp46 and T-bet expression (Supplementary Fig. 5c). Furthermore, MHCII$^+$RORγt$^+$ ILCs were found in lymphoid tissues at steady state (Supplementary Fig. 6), exhibited homogeneous expression of CD127, CD90.2, CD25, CCR6, c-kit and CD44, and heterogeneous expression of Sca-1 and CD4 (Supplementary Fig. 7a) and produced IL-22, but not IL-17A or IFN-γ, in response to IL-23 stimulation (Supplementary Fig. 7b).

To interrogate the functional capacity of MHCII$^+$ ILCs, cells were sort-purified and cultured with DQ-ovalbumin (DQ-OVA), a self-quenching conjugate of ovalbumin that fluoresces upon proteolytic degradation. MHCII$^+$ ILCs exhibited an increase in fluorescence intensity comparable to CD11c$^+$MHCII$^+$ dendritic cells after incubation with DQ-OVA (Fig. 2c), indicative of an ability to acquire and degrade antigens. Sort-purified ILCs were also cultured with green fluorescent protein (GFP)-labelled E-alpha (Eα) protein and stained with an antibody specific for Eα-derived $E\alpha_{52-68}$ peptide bound to I–A^b molecules (Y-Ae). MHCII$^+$ ILCs incubated with GFP–Eα exhibited positive GFP fluorescence and staining for Y-Ae at levels comparable to those of CD11c$^+$MHCII$^+$ dendritic cells (Fig. 2d), demonstrating that ILCs can process exogenous protein and present peptide antigen in the context of MHCII. However, in contrast to OVA-pulsed dendritic cells that induced multiple rounds of ovalbumin-specific CD4$^+$ T-cell proliferation, OVA-pulsed ILCs failed to induce ovalbumin-specific CD4$^+$ T-cell proliferation (Fig. 2e). Consistent with this, MHCII$^+$RORγt$^+$ ILCs lacked expression of the classical co-stimulatory molecules CD40, CD80 and CD86, relative to dendritic cells (Fig. 2f). Antigen presentation in the absence of co-stimulatory molecules has been proposed to limit T-cell responses[22], suggesting that MHCII$^+$RORγt$^+$ ILCs may negatively regulate CD4$^+$

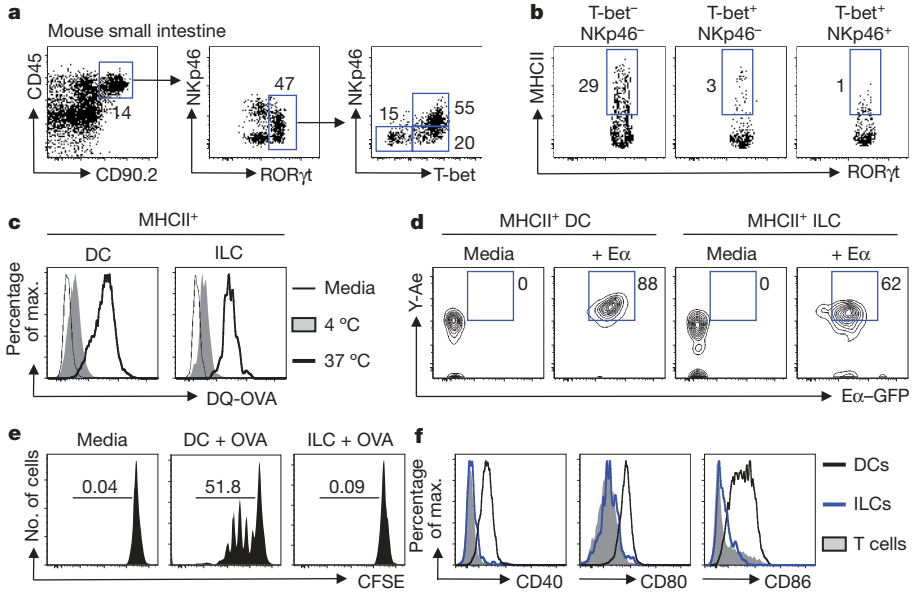

Figure 2 | T-bet⁻NKp46⁻RORγt⁺ ILCs express MHCII and process and present antigen, but do not induce T-cell proliferation. **a**, **b**, Gating strategy (**a**) and expression of MHCII (**b**) in group 3 ILC subsets in the small intestine of naive mice. **c**, **d**, Sorted cell populations were cultured in the absence (thin line) or presence of DQ-OVA at 4 °C (shaded) or 37 °C (thick line) (**c**) or cultured in the absence (media) or presence of Eα–GFP protein and stained with Y-Ae antibody (**d**). **e**, Sort-purified CFSE-labelled CD4$^+$ T cells from OT-II mice were cultured in the presence of media alone or with OVA-pulsed dendritic cells (DCs) or OVA-pulsed ILCs. **f**, Expression of co-stimulatory molecules on dendritic cells (black line), ILCs (blue line) or T cells (shaded) from the mesenteric lymph nodes of naive mice. Data are representative of 2–3 independent experiments containing 2–5 mice per group or 2–3 *in vitro* replicates.

T-cell responses *in vivo*. To test this, ILCs were pulsed with the commensal bacteria-derived antigen CBir1 (ref. 23) and co-transferred with CBir1-specific transgenic T cells into naive congenic mice, before systemic challenge with peptide (Supplementary Fig. 8a). Mice that received a co-transfer of CBir1-specific T cells with peptide-pulsed ILCs exhibited a reduced population expansion of transferred T cells and decreased antigen-specific IFN-γ production relative to transfer of T cells alone (Supplementary Fig. 8b–d), suggesting that antigen presentation by ILCs limits CD4$^+$ T-cell responses *in vivo*.

To investigate further the ability of MHCII$^+$RORγt$^+$ ILCs to regulate adaptive immune cell responses, mice were generated with a RORγt$^+$ ILC-intrinsic deletion of MHCII (MHCII$^{\Delta ILC}$) by crossing

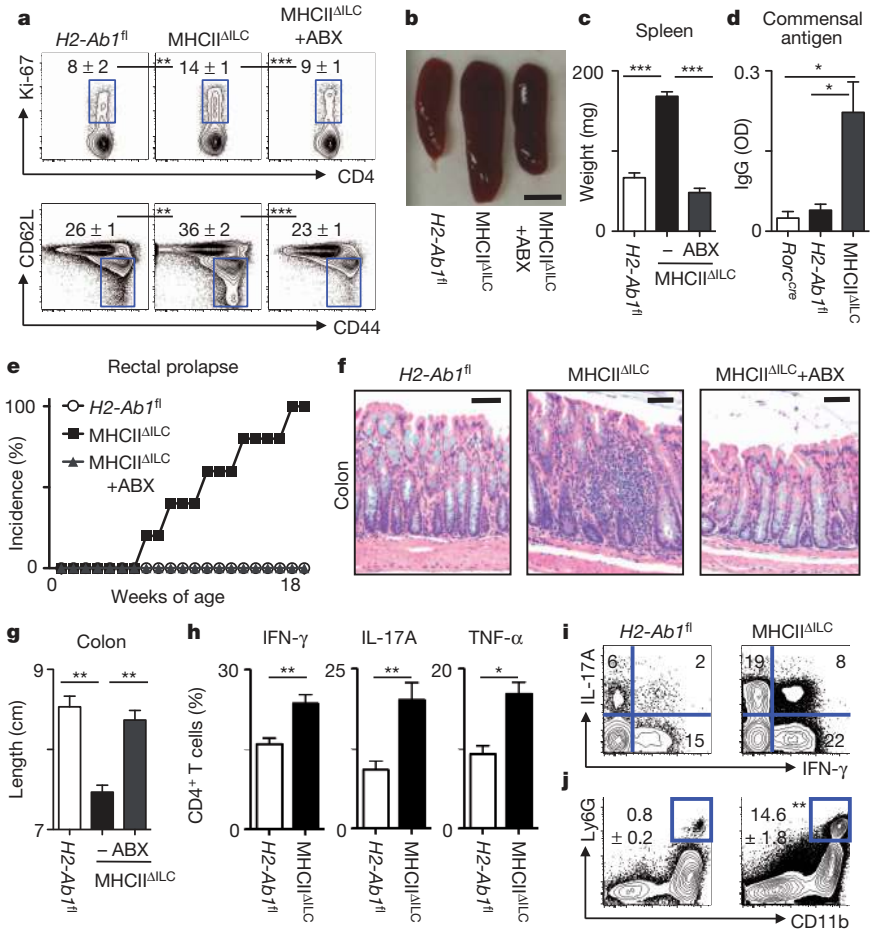

Figure 3 | Loss of RORγt$^+$ ILC-intrinsic MHCII expression results in commensal bacteria-dependent intestinal inflammation. **a**–**d**, Age- and sex-matched mice were examined for the frequency of splenic Ki-67$^+$CD4$^+$ T cells (top) and CD44^{high}CD62L^{low}CD4$^+$ T cells (bottom) (**a**), spleen size (**b**), spleen weight (**c**) and relative serum IgG specific to commensal bacteria (**d**). Scale bar, 0.5 cm (**b**). Flow cytometry plots are gated on live CD4$^+$CD3$^+$ T cells (**a**). **e**–**g**, Mice were examined for incidence of rectal prolapse (**e**), histological changes in haematoxylin and eosin stained sections of the terminal colon (**f**) and colon length (**g**). Scale bars, 25 μm (**f**). Antibiotics (ABX) were continuously administered in the drinking water of selected mice at weaning until 8–18 weeks of age. **h**–**j**, Frequency of total IFN-γ$^+$, IL-17A$^+$ and TNF-α$^+$ CD4$^+$ T cells (**h**) and IL-17A$^+$IFN-γ$^+$CD4$^+$ T cells (**i**) in the colons after a brief *ex vivo* stimulation and frequency of CD11b$^+$ Ly6G$^+$ neutrophils in colonic lamina propria (**j**). Data are representative of three independent experiments containing 3–5 mice per group. Results are shown as the means ± s.e.m. $^*P < 0.05$, $^{**}P < 0.01$, $^{***}P < 0.001$ (two-tailed Student' *t*-test).

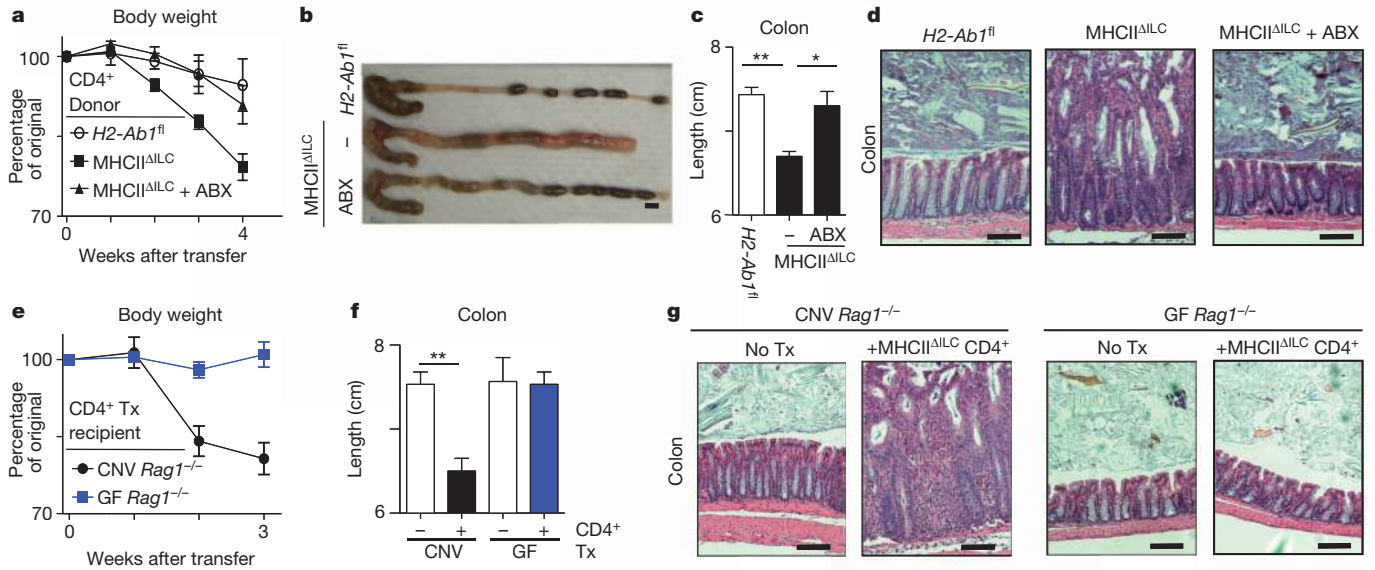

Figure 4 | RORγt$^+$ ILC-intrinsic MHCII regulates pathological CD4$^+$ T-cell responses to commensal bacteria. **a**–**g**, *Rag1*$^{-/-}$ mice received CD4$^+$ T cells sort-purified from defined donor mouse strains (**a**–**d**), or conventional (CNV) and germ-free (GF) *Rag1*$^{-/-}$ mice received sort-purified CD4$^+$ T cells from MHCII$^{\Delta ILC}$ mice via adoptive transfer (± Tx) (**e**–**g**). Recipients were examined for changes in weight (**a**, **e**), macroscopic colon pathology (**b**), colon length (**c**, **f**) and histological changes in the terminal colon (**d**, **g**). Scale bars, 0.5 cm (**b**) or 25 μm (**d**, **g**). In some experiments, antibiotics (ABX) were administered in the drinking water of donor mice from weaning (**a**–**d**). Data are representative of two independent experiments containing 3–5 mice per group. Results are shown as the means ± s.e.m. $*P < 0.05$, $**P < 0.01$ (two-tailed Student's *t*-test).

mice with a floxed *H2-Ab1* gene (*H2-Ab1*^{fl}) with mice expressing Cre recombinase under the control of the *Rorc* promoter (*Rorc*^{cre}) (Supplementary Fig. 9a). Given that *Rorc* is expressed only by T cells and ILCs[15,16] and that murine T cells do not express MHCII[24], this permitted selective genetic deletion of MHCII in RORγt$^+$ ILCs in the presence of an intact adaptive immune system. Consistent with this, MHCII$^{\Delta ILC}$ mice exhibited a selective loss of MHCII expression on RORγt$^+$ ILCs, whereas B cells, dendritic cells and macrophages retained comparable expression levels of MHCII relative to control *H2-Ab1*^{fl} mice (Supplementary Fig. 9b). MHCII$^{\Delta ILC}$ mice also had comparable peripheral numbers of lymph nodes and Peyer's patches, frequencies of ILCs and production of ILC-derived IL-22 (Supplementary Fig. 9c, d) as compared to control mice. However, MHCII$^{\Delta ILC}$ mice did exhibit significantly increased frequencies of peripheral Ki-67$^+$CD4$^+$ T cells and CD44^{high}CD62L^{low}CD4$^+$ T cells, increased spleen size and weight and a significant increase in commensal bacteria-specific serum IgG, which were abrogated upon oral administration of antibiotics (Fig. 3a–d). Thus, loss of ILC-intrinsic MHCII expression recapitulated the phenotype observed after genetic or antibody-mediated depletion of ILCs (Fig. 1a–d and Supplementary Fig. 1a–d) identifying a critical role for MHCII$^+$ ILCs in regulating T-cell responses to commensal bacteria.

Inappropriate host inflammatory responses to commensal bacteria are associated with the pathogenesis and progression of numerous chronic human diseases[3,11–13], therefore MHCII$^{\Delta ILC}$ mice were examined at various ages for signs of inflammation. MHCII$^{\Delta ILC}$ mice were observed to develop rectal prolapse, beginning at approximately 8 weeks of age and reaching a 100% incidence by 18 weeks of age (Fig. 3e). Further examination revealed that MHCII$^{\Delta ILC}$ mice exhibited intestinal inflammation characterized by crypt elongation, loss of normal architecture and significantly decreased colon length (Fig. 3f, g). Intestinal inflammation in MHCII$^{\Delta ILC}$ mice could be prevented by continuous administration of antibiotics (Fig. 3e–g), demonstrating a critical role for commensal bacteria in the development of disease. Moreover, MHCII$^{\Delta ILC}$ mice exhibited significantly elevated frequencies of IFN-γ$^+$, IL-17A$^+$ and TNF-α$^+$ CD4$^+$ T cells in the colon (Fig. 3h), including CD4$^+$ T cells that co-produced IFN-γ and IL-17A (Fig. 3i), which was associated with significant recruitment of neutrophils into the colonic lamina propria (Fig. 3j). Further phenotypic and functional analyses suggested that the increased pro-inflammatory CD4$^+$ T-cell responses and intestinal inflammation that developed in the absence of ILC-intrinsic MHCII were not the result of impaired regulatory T-cell function or regulatory cytokine production (Supplementary Fig. 10), altered thymic selection (Supplementary Fig. 11) or commensal microflora dysbiosis (Supplementary Fig. 12). Collectively, these data suggest that ILCs directly limit commensal bacteria-responsive CD4$^+$ T cells through MHCII-dependent interactions.

To determine whether dysregulated CD4$^+$ T-cell responses to commensal bacteria directly promoted intestinal inflammation observed in MHCII$^{\Delta ILC}$ mice, sort-purified CD4$^+$ T cells from control *H2-Ab1*^{fl} mice or MHCII$^{\Delta ILC}$ mice were transferred into *Rag1*$^{-/-}$ mice. In comparison to *Rag1*$^{-/-}$ recipients receiving CD4$^+$ T cells from control mice, *Rag1*$^{-/-}$ recipients receiving CD4$^+$ T cells from MHCII$^{\Delta ILC}$ mice exhibited rapid and substantial weight loss (Fig. 4a), colonic shortening, macroscopic intestinal thickening and severe intestinal inflammation characterized by crypt elongation, loss of normal architecture and inflammatory cell infiltrates (Fig. 4b–d). Critically, oral administration of antibiotics to MHCII$^{\Delta ILC}$ donor mice before CD4$^+$ T-cell isolation abrogated the ability of CD4$^+$ T cells to elicit wasting disease and intestinal inflammation in naive *Rag1*$^{-/-}$ recipients (Fig. 4a–d). Similarly, germ-free *Rag1*$^{-/-}$ recipients of CD4$^+$ T cells from MHCII$^{\Delta ILC}$ mice did not develop wasting disease or intestinal inflammation in comparison to conventional *Rag1*$^{-/-}$ recipients (Fig. 4e–g). Therefore, in the absence of RORγt$^+$ ILC-intrinsic MHCII, commensal bacteria are required for both the development of pathological CD4$^+$ T-cell responses and for the onset of wasting disease and intestinal inflammation.

Collectively, these data identify a previously unrecognized role for RORγt$^+$ ILCs in maintaining intestinal homeostasis by limiting pathological CD4$^+$ T-cell responses to commensal bacteria through MHCII-dependent interactions (Supplementary Fig. 13). MHCII expression was found to be restricted to a subset of CCR6$^+$RORγt$^+$ ILCs that lack T-bet and IFN-γ expression and thus, are phenotypically and functionally distinct from RORγt$^+$ ILC populations that have been associated with promoting intestinal inflammation in murine models and inflammatory bowel disease patients[2,11]. Rather, MHCII$^+$RORγt$^+$

ILCs are more similar to IL-22-producing ILC populations previously shown to promote tissue protection[3,5,8,12–14]. In a developmental context, it is remarkable that RORγt$^+$ ILCs are the first cells of the immune system to colonize the neonatal intestine and gut-associated lymphoid tissues[15,25,26]. Therefore, ILCs may have a critical role not only in promoting lymphoid organogenesis and cytokine-mediated epithelial cell barrier integrity but also in regulating adaptive immune cell responses to newly colonizing commensal bacteria. It may also be advantageous for ILCs to modulate commensal bacteria-specific T cells as, in contrast to professional antigen presenting cells, murine ILCs lack expression of TLRs, conventional co-stimulatory molecules and do not produce cytokines that regulate T-cell differentiation[1,8,10,25]. The demonstration that ILCs regulate adaptive immune cell responses to commensal bacteria through a MHCII-dependent mechanism may be of importance in understanding the pathogenesis of numerous chronic human diseases associated with inflammatory host immune responses to commensal bacteria.

METHODS SUMMARY

MHCII$^{\Delta ILC}$ mice were generated by crossing *H2-Ab1*^{fl} mice with *Rorc*^{cre} mice. *H2-Ab1*^{fl} littermates were used as controls for all experiments. Intestinal lamina propria and lymphoid tissue cell suspensions were isolated as previously described[3,7]. In some experiments mice were treated with antibiotics as previously described[3]. Commensal bacteria-derived antigen-specific enzyme-linked immunosorbent assays (ELISAs) were performed by coating 96-well plates with 5 μg ml^{-1} crude commensal bacteria antigen, prepared by isolation of faecal contents and sequential homogenization and sonication. ILCs were identified by exclusion of lineage-positive cells by staining with fluorochrome-conjugated antibodies against CD3, CD5, CD8α, CD11c, NK1.1 and B220 and by positive expression of CD45 and CD90.2 or by expression of GFP in RORγt–eGFP mice. Sort-purified ILCs and dendritic cells were assessed for antigen processing and presentation capacity by culturing cells with 10 μg ml^{-1} DQ-OVA for 3 h or by culturing for 3 h with 50 μg ml^{-1} GFP-labelled E-alpha protein, followed by subsequent staining with an antibody recognizing Eα_{52-68} peptide bound to I–A^b. Lymphocyte populations (≥95%) were sort-purified using a BD FACS Aria II. CD4$^+$ T cells were adoptively transferred to conventional or germ-free *Rag1*$^{-/-}$ recipients via intravenous injection. Data are represented as the mean ± s.e.m. and statistical significance was determined by the Student's *t*-test.

Full Methods and any associated references are available in the online version of the paper.

Received 4 November 2012; accepted 2 May 2013.
Published online 22 May 2013.

1. Spits, H. & Cupedo, T. Innate lymphoid cells: emerging insights in development, lineage relationships, and function. *Annu. Rev. Immunol.* **30,** 647–675 (2012).
2. Buonocore, S. *et al.* Innate lymphoid cells drive interleukin-23-dependent innate intestinal pathology. *Nature* **464,** 1371–1375 (2010).
3. Sonnenberg, G. F. *et al.* Innate lymphoid cells promote anatomical containment of lymphoid-resident commensal bacteria. *Science* **336,** 1321–1325 (2012).
4. Cella, M. *et al.* A human natural killer cell subset provides an innate source of IL-22 for mucosal immunity. *Nature* **457,** 722–725 (2009).
5. Sawa, S. *et al.* RORγt$^+$ innate lymphoid cells regulate intestinal homeostasis by integrating negative signals from the symbiotic microbiota. *Nature Immunol.* **12,** 320–326 (2011).
6. Lochner, M. *et al.* Microbiota-induced tertiary lymphoid tissues aggravate inflammatory disease in the absence of RORγt and LTi cells. *J. Exp. Med.* **208,** 125–134 (2011).
7. Sonnenberg, G. F., Monticelli, L. A., Elloso, M. M., Fouser, L. A. & Artis, D. CD4(+) lymphoid tissue-inducer cells promote innate immunity in the gut. *Immunity* **34,** 122–134 (2011).
8. Sonnenberg, G. F. & Artis, D. Innate lymphoid cell interactions with microbiota: implications for intestinal health and disease. *Immunity* **37,** 601–610 (2012).
9. Spits, H. *et al.* Innate lymphoid cells—a proposal for uniform nomenclature. *Nature Rev. Immunol.* **13,** 145–149 (2013).
10. Walker, J. A., Barlow, J. L. & McKenzie, A. N. Innate lymphoid cells—how did we miss them? *Nature Rev. Immunol.* **13,** 75–87 (2013).
11. Geremia, A. *et al.* IL-23-responsive innate lymphoid cells are increased in inflammatory bowel disease. *J. Exp. Med.* **208,** 1127–1133 (2011).
12. Takayama, T. *et al.* Imbalance of NKp44$^+$NKp46$^-$ and NKp44$^-$NKp46$^+$ natural killer cells in the intestinal mucosa of patients with Crohn's disease. *Gastroenterology* **139,** 882–892 (2010).
13. Ciccia, F. *et al.* Interleukin-22 and IL-22-producing NKp44$^+$ NK cells in the subclinical gut inflammation of patients with ankylosing spondylitis. *Arthritis Rheum.* **64,** 1869–1878 (2011).
14. Sonnenberg, G. F., Fouser, L. A. & Artis, D. Border patrol: regulation of immunity, inflammation and tissue homeostasis at barrier surfaces by IL-22. *Nature Immunol.* **12,** 383–390 (2011).
15. Eberl, G. & Littman, D. R. Thymic origin of intestinal αβ T cells revealed by fate mapping of RORγt$^+$ cells. *Science* **305,** 248–251 (2004).
16. Sawa, S. *et al.* Lineage relationship analysis of RORγt$^+$ innate lymphoid cells. *Science* **330,** 665–669 (2010).
17. Monticelli, L. A. *et al.* Innate lymphoid cells promote lung-tissue homeostasis after infection with influenza virus. *Nature Immunol.* **12,** 1045–1054 (2011).
18. Reynders, A. *et al.* Identity, regulation and *in vivo* function of gut NKp46$^+$RORγt$^+$ and NKp46$^+$RORγt$^-$ lymphoid cells. *EMBO J.* **30,** 2934–2947 (2011).
19. Yosef, N. *et al.* Dynamic regulatory network controlling T17 cell differentiation. *Nature* **496,** 461–468 (2013).
20. Bezman, N. A. *et al.* Molecular definition of the identity and activation of natural killer cells. *Nature Immunol.* **13,** 1000–1009 (2012).
21. Klose, C. S. *et al.* A T-bet gradient controls the fate and function of CCR6-RORγt$^+$ innate lymphoid cells. *Nature* **494,** 261–265 (2013).
22. Schwartz, R. H. T cell anergy. *Annu. Rev. Immunol.* **21,** 305–334 (2003).
23. Cong, Y., Feng, T., Fujihashi, K., Schoeb, T. R. & Elson, C. O. A dominant, coordinated T regulatory cell-IgA response to the intestinal microbiota. *Proc. Natl Acad. Sci. USA* **106,** 19256–19261 (2009).
24. Benoist, C. & Mathis, D. Regulation of major histocompatibility complex class-II genes: X, Y and other letters of the alphabet. *Annu. Rev. Immunol.* **8,** 681–715 (1990).
25. Mebius, R. E., Rennert, P. & Weissman, I. L. Developing lymph nodes collect CD4+CD3- LTbeta+ cells that can differentiate to APC, NK cells, and follicular cells but not T or B cells. *Immunity* **7,** 493–504 (1997).
26. Eberl, G. *et al.* An essential function for the nuclear receptor RORγt in the generation of fetal lymphoid tissue inducer cells. *Nature Immunol.* **5,** 64–73 (2004).

Supplementary Information is available in the online version of the paper.

Acknowledgements We thank members of the Sonnenberg and Artis laboratories for discussions and critical reading of the manuscript. We also thank H. L. Ma, L. A. Fouser, S. Olland, R. Zollner, K. Lam and A. Root at Pfizer for critical discussions, valuable advice and the preparation of IL-22 antibodies; M. M. Elloso at Janssen Research and Development for critical discussions, valuable advice and the preparation of IL-17 and IL-23 antibodies; and M.S. Marks for providing the E-alpha protein and Y-Ae antibody. The research is supported by the National Institutes of Health (AI061570, AI087990, AI074878, AI095776, AI102942, AI095466, AI095608 and AI097333 to D.A.; T32-AI055428 to L.A.M.; DK071176 to C.O.E.; and DP5OD012116 to G.F.S.), the Crohn's and Colitis Foundation of America (to D.A.) and the Burroughs Wellcome Fund Investigator in Pathogenesis of Infectious Disease Award (to D.A.). We also thank the Matthew J. Ryan Veterinary Hospital Pathology Lab, the National Institute of Diabetes and Digestive and Kidney Disease Center for the Molecular Studies in Digestive and Liver Disease Molecular Pathology and Imaging Core (P30DK50306), the Penn Microarray Facility and the Abramson Cancer Center Flow Cytometry and Cell Sorting Resource Laboratory (partially supported by NCI Comprehensive Cancer Center Support Grant (2-P30 CA016520)) for technical advice and support. Human tissue samples were provided by the Cooperative Human Tissue Network, which is funded by the National Cancer Institute.

Author Contributions M.R.H., L.A.M., T.C.F., D.A. and G.F.S. designed and performed the research. C.G.K.Z. performed analyses of microarray data. A.C., J.M.A. and E.J.W. performed the microarray of naive CD4$^+$ T cells. S.G., R.S. and F.D.B. provided advice, performed and analysed 454 pyrosequencing of intestinal commensal bacteria. A.R.M. assisted with reagents and advice for antigen presentation assays. H.-L.M., P.A.K., C.O.E. and G.E. provided essential mouse strains, valuable advice and technical expertise for these studies. M.R.H., L.A.M., T.C.F., D.A. and G.F.S. analysed the data. M.R.H., D.A. and G.F.S. wrote the manuscript.

Author Information Reprints and permissions information is available at www.nature.com/reprints. The authors declare no competing financial interests. Readers are welcome to comment on the online version of the paper. Correspondence and requests for materials should be addressed to G.F.S. (gfield@mail.med.upenn.edu).

METHODS

Mice, antibiotics and use of monoclonal antibodies *in vivo*. C57BL/6 mice, C57BL/6 *Rag1*$^{-/-}$, C57BL/6 CD90.1 and C57BL/6 *Rorc*$^{gfp/gfp}$ mice were purchased from the Jackson Laboratory, bred and maintained at the University of Pennsylvania. C57BL/6 *Il17a*$^{-/-}$ mice were provided by Y. Iwakura (University of Tokyo), C57BL/6 *Il22*$^{-/-}$ mice were provided by Pfizer, *Il23a*$^{-/-}$ mice were provided by Janssen Research & Development LLC, *H2-Ab1*^{fl} mice were provided by P. A. Koni, tissues from CBir1 TCR transgenic mice were provided by C. O. Elson, and *Rorc*^{cre} mice and *Rorc(γt)-Gfp*^{TG} were provided by G. Eberl. All mice were maintained in specific pathogen-free facilities at the University of Pennsylvania. Germ-free C57BL/6 and C57BL/6 *Rag1*$^{-/-}$ mice were provided by the University of Pennsylvania Gnotobiotic Mouse Facility. CD90-disparate *Rag*1$^{-/-}$ chimaeras were constructed as previously described[3,7]. All protocols were approved by the University of Pennsylvania Institutional Animal Care and Use Committee (IACUC), and all experiments were performed according to the guidelines of the University of Pennsylvania IACUC. A previously described cocktail of antibiotics was continuously administered via drinking water for defined periods of time[3,27]. Anti-CD90.2 monoclonal antibody (30H12) was purchased from BioXCell. Anti-IL-22 monoclonal antibodies, IL22-01 (neutralizing) and IL22-02 (mouse cytokine detection) were developed by Pfizer. Anti-IL-17A monoclonal antibody (CNTO 8096) and anti-IL-23p19 monoclonal antibody (CNTO 6163) were developed by Janssen Research & Development, LLC. Anti-IL-17RA monoclonal antibody was developed by Amgen Inc. Neutralizing or depleting monoclonal antibodies were administered intraperitoneally every 3 days at a dose of 250 μg per mouse starting on day 0 and ending on day 14.

Murine tissue isolation and flow cytometry. Spleens, lymph nodes and Peyer's patches were harvested, and single-cell suspensions were prepared at necropsy as previously described[3,7]. For intestinal lamina propria lymphocyte preparations, intestines were isolated, attached fat removed and tissues cut open longitudinally. Luminal contents were removed by shaking in cold PBS. Epithelial cells and intraepithelial lymphocytes were removed by shaking tissue in stripping buffer (1 mM EDTA, 1 mM DTT and 5% FCS) for 30 min at 37 °C. The lamina propria layer was isolated by digesting the remaining tissue in 0.5 mg ml^{-1} collagenase D (Roche) and 20 μg ml^{-1} DNase I (Sigma-Aldrich) for 30 min at 37 °C.

For flow cytometric analyses, cells were stained with antibodies to the following markers: anti-NK1.1 (clone PK136, eBioscience), anti-CD3 (clone 145-2C11, eBioscience), anti-CD5 (clone 53-7.3, eBioscience), anti-CD90.2 (clone 30-H12, BioLegend), anti-CD127 (clone A7R34, eBioscience), anti-CD11c (clone N418, eBioscience), anti-F4/80 (clone BM8, eBioscience), anti-CD4 (clone GK1.5, Abcam), anti-CD8 (clone 53-6.7, eBioscience), anti-B220 (clone RA3-6B2, eBioscience), anti-CD25 (clone eBio3C7, eBioscience), anti-MHCII (clone M5/114.15.2, eBioscience), anti-CD44 (clone IM7, eBioscience), anti-CD62L (clone MEL-14, eBioscience), anti-CD45 (clone 30-F11, eBioscience), anti-NKp46 (clone 29A1.4, eBioscience), anti-CD11b (clone M1/70, eBioscience), anti-CD117 (c-kit) (clone 2B8, eBioscience), anti-Sca-1 (clone D7, eBioscience), anti-CD40 (clone 1C10, eBioscience), anti-CD80 (clone 16-10A1, eBioscience), anti-CD86 (clone GL1, BD Biosciences), anti-Ly6G (clone 1A8, BioLegend) and anti-CCR6 (clone 29-2L17, BioLegend). For intracellular staining, cells were fixed and permeabilized using a commercially available kit (eBioscience) and stained with anti-RORγt (clone B2D, eBioscience), anti-FoxP3 (clone FJK016s, eBioscience), anti-T-bet (clone eBio-4B10, eBioscience), anti-GATA-3 (clone TWAJ, eBioscience) or anti-Ki-67 (clone B56, BD Biosciences). For cytokine production, cells were stimulated *ex vivo* by incubation for 4 h with 50 ng ml^{-1} PMA, 750 ng ml^{-1} ionomycin, 10 μg ml^{-1} brefeldin A (all obtained from Sigma-Aldrich) or 50 ng ml^{-1} rIL-23 (eBioscience) and 10 μg ml^{-1} brefeldin A. Cells were fixed and permeabilized as indicated above and stained with IL22-02 (Pfizer) conjugated to Alexa Fluor 647 or Alexa Fluor 488 according to the manufacturer's instructions (Molecular Probes), anti-IL-17A (clone eBioTC11-18H10.1, eBioscience), anti-IFN-γ (clone XMG1.2, eBioscience) and anti-TNF-α (clone MP6-XT22, eBioscience). Dead cells were excluded from analysis using a violet viability stain (Invitrogen). T-cell Vβ chain usage was assessed using a commercial mouse Vβ TCR screening panel (BD Biosciences). Flow cytometry data collection was performed on a LSR II (BD Biosciences) and cell sorting performed on an Aria II (BD Biosciences). Data were analysed using FlowJo software (Tree Star Inc.).

Human intestinal samples and flow cytometry. Human intestinal tissues from the ileum were obtained from the Cooperative Human Tissue Network. Single cell suspensions from intestinal tissues were obtained by cutting tissues into small pieces and incubating for 1–2 h at 37 °C with shaking in stripping buffer (1 mM EDTA, 1 mM DTT and 5% FCS) to remove the epithelial layer. Supernatants were then discarded, and the lamina propria fraction was obtained by incubating the remaining tissue for 1–2 h at 37 °C with shaking in collagenase solution. Remaining tissues were then mechanically dissociated, filtered through a wire mesh tissue sieve, and lymphocytes were subsequently separated by Ficoll gradient.

For flow cytometry, cells were stained with antibodies to the following markers: anti-CD3 (clone UCHT1, eBioscience), anti-CD56 (clone CMSSB, eBioscience), anti-CD19 (clone 2H7, eBioscience), anti-HLA-DR (clone LN3, eBioscience), anti-CD127 (clone A019D5, Biolegend). For intracellular staining, cells were fixed and permeabilized using a commercially available kit (eBioscience) and stained with anti-RORγt (clone AFKJS-9, eBioscience) and anti-IL-22 (clone 22URTI, eBioscience). Dead cells were excluded from analysis using a viability stain (Invitrogen). Flow cytometry data was collected using a LSR II (BD Biosciences). Data were analysed using FlowJo software (Tree Star Inc.).

Histological sections. Tissue samples from the intestines of mice were fixed with 4% paraformaldehyde, embedded in paraffin, and 5 μm sections were stained with haematoxylin and eosin.

Microarray and DAVID pathway analysis. Microarray gene expression profiling and data normalization for group 2 ILCs (sorted Lineage$^-$, CD90.2$^+$, CD25$^+$ ILCs from the lungs of naive C57BL/6 mice), group 3 ILCs (Lineage$^-$, CD90.2$^+$, CD4$^+$ ILCs from the spleens of naive C57BL/6 mice) and naive splenic CD4$^+$ T cells were performed as previously described (GEO accession numbers; GSE46468 and GSE30437), data were RMA-normalized and SAM analysis was performed[17]. Additional microarray gene expression profiling were obtained from GEO for previously published studies of *in vitro* polarized T_H17 cells (GSM1074979, GSM1075001 and GSM1075002)[19], splenic NK cells (GSM538315, GSM538316 and GSM538317)[20] and subsets of RORγ$^+$ ILCs isolated from naive murine small intestine (GSM739586, GSM739591, GSM739588, GSM739593, GSM739589 and GSM739594)[18]. GEO data sets were batch-corrected to existing microarray gene expression profiles using ComBat[28]. Differentially expressed genes in the transcriptional profiles of specified groups were uploaded to the Database for Annotation, Visualization and Integrated Discovery (DAVID, http://david.abcc.ncifcrf.gov/)[29] and analysed as previously described[17] using the Fisher's exact test to identify significantly enriched Gene Ontology (GO, http://www.geneontology.org) terms[29]. Heat maps displaying key genes were generated using Mayday software[30].

Antigen processing and presentation analyses. 2×10^3 sort-purified CD11c$^+$MHCII$^+$ dendritic cells and lineage$^-$CD127$^+$c-kit$^+$MHCII$^+$ ILCs were cultured with 10 μg ml^{-1} DQ-OVA (Molecular Probes) at 4 °C or 37 °C for 3 h, extensively washed and fluorescence assessed via flow cytometry. Alternatively, antigen processing and presentation were assessed using a previously defined self-antigen E-alpha[31]. Briefly, 2×10^3 sort-purified dendritic cells and ILCs were pulsed for 3 h in complete media with 50 μg ml^{-1} GFP-labelled E-alpha protein, extensively washed and stained with a biotin-conjugated antibody recognizing $E\alpha_{52-68}$ peptide bound to I-A^b (clone Yae, eBioscience) followed by a streptavidin APC (eBioscience) and uptake of antigen and peptide-MHCII complex presentation assessed via flow cytometry. In some assays 2×10^3 sort-purified dendritic cells or ILCs were pulsed with 50 μg ovalbumin for 2 h before incubation with 2×10^4 sort-purified CFSE-labelled OT-II T cells. Cell co-cultures were incubated for 72 h before analysis via flow cytometry.

T-cell adoptive transfer. 2×10^6 CD4$^+$CD3$^+$ T cells were sorted from the spleen and mesenteric lymph node of control or experimental mice to a purity >97% and transferred intravenously to naive C57BL/6 *Rag1*$^{-/-}$ recipient mice (GF or CNV). Weights of recipient mice were monitored through the progression of the experiment.

CBir1-specific T-cell transfers. 1×10^6 CBir1 TCR transgenic T cells were transferred into congenically marked hosts with or without co-transfer of 8×10^3 sort-purified ILCs (lineage$^-$ CD127$^+$ c-kit$^+$) pulsed with 1 μg ml^{-1} $CBir1_{456-475}$ peptide. Twenty-four hours later mice were administered 50 μg $CBir1_{456-475}$ peptide intraperitoneally and 72 h later mice were euthanized and the presence of CBir1 TCR transgenic T cells was quantified in the spleen. IFN-γ production was quantified by culturing 1×10^6 splenocytes in the presence of 1 μg ml^{-1} $CBir1_{456-475}$ peptide for 48 h.

Regulatory T-cell suppression assay. CD11c$^+$ dendritic cells, naive CD4$^+$CD25$^-$ CD45RB^{hi} T effector (T_{eff}) cells and CD4$^+$CD25$^+$CD45RB$^-$ regulatory T cells (T_{reg}) cells were sort-purified from the spleen and mesenteric lymph node of MHCII$^{\Delta ILC}$ mice and littermate controls. Sort-purified T_{reg} cells were found to be at least 98% FoxP3$^+$. Dendritic cells were plated at 5×10^3 per well in the presence or absence of 1 μg ml^{-1} soluble purified anti-CD3 (clone 145-2C11, BD Biosciences). T_{eff} cells were CFSE labelled and added to wells containing dendritic cells at 2.5×10^4 alone, or with T_{reg} at a ratio of 1:0, 1:2, 1:4, 1:8 and 1:16. After 3 days culture at 37 °C/5% CO_2, cell-culture supernatants were harvested and T_{eff} proliferation was measured by CFSE dilution via flow cytometry. T_{reg} suppression was calculated by gating on T effector cells and quantifying the percentage of CFSE-dim in comparison to cells cultured in the absence of T_{reg} cells.

Quantitative real-time PCR. RNA was isolated from whole colon tissue that was homogenized and snap frozen in Trizol reagent (Invitrogen). RNA was isolated as per the manufacturer's instructions and cDNA generated using Superscript reverse transcription (Invitrogen). Real-time PCR was performed on cDNA using

SYBR green chemistry (Applied Biosystems) using commercially available primer sets (QIAGEN). Reactions were run on a real-time PCR system (ABI7500; Applied Biosystems). Samples were normalized to β-actin and displayed as a fold change as compared to control mice.

Commensal bacteria-specific ELISA. Colonic faecal contents were homogenized and briefly centrifuged at 1,000 r.p.m. to remove large aggregates, and the resulting supernatant was washed with sterile PBS twice by centrifuging for 1 min at 8,000 r.p.m. On the last wash, bacteria were re-suspended in 2 ml ice-cold PBS and sonicated on ice. Samples were then centrifuged at 20,000*g* for 10 min, and supernatants recovered for a crude commensal bacteria antigen preparation. For measurement of serum antibodies by ELISA, 5 μg ml^{-1} commensal bacteria antigen was coated on 96-well plates, and sera were incubated in doubling dilutions. Antigen-specific IgG was detected using an anti-mouse IgG-HRP antibody (BD Biosciences). Plates were developed with TMB peroxidase substrate (KPL), and optical densities measured using a plate spectrophotometer.

Microbiota transfer to germ-free mice. The caeca of MHCII$^{\Delta ILC}$ mice and littermate controls were opened under aseptic conditions and caecal contents re-suspended in sterile PBS. Germ-free C57BL/6 mice were then orally gavaged with 200 μl of caecal content suspension and subsequently monitored over the course of 6 weeks for signs of disease and rectal prolapse before death.

Pyrosequencing. DNA from luminal contents from the large intestine of mice was obtained using the QIAamp DNA Stool mini kit (Qiagen). DNA samples were amplified using the V1-V2 region primers targeting bacterial 16S genes and sequenced using 454/Roche Titanium technology. Sequence analysis was carried out using the QIIME pipeline[32] for co-housed cohorts of *H2-Ab1*^{fl} and MHCII$^{\Delta ILC}$ mice.

Statistical analysis. Results represent the mean ± s.e.m. Statistical significance was determined by the Student's *t*-test ($*P < 0.05$; $**P < 0.01$; $***P < 0.001$).

27. Abt, M. C. *et al.* Commensal bacteria calibrate the activation threshold of innate antiviral immunity. *Immunity* **37,** 158–170 (2012).
28. Johnson, W. E., Li, C. & Rabinovic, A. Adjusting batch effects in microarray expression data using empirical Bayes methods. *Biostatistics* **8,** 118–127 (2007).
29. Huang, D. W. *et al.* Extracting biological meaning from large gene lists with DAVID. *Curr. Protoc. Bioinform.* Ch. 13, Unit 13 11 (2009).
30. Battke, F., Symons, S. & Nieselt, K. Mayday–integrative analytics for expression data. *BMC Bioinformatics* **11,** 121 (2010).
31. Murphy, D. B. *et al.* A novel MHC class II epitope expressed in thymic medulla but not cortex. *Nature* **338,** 765–768 (1989).
32. Caporaso, J. G. *et al.* QIIME allows analysis of high-throughput community sequencing data. *Nature Methods* **7,** 335–336 (2010).